Precise Positioning of Enzymes within Hierarchical Polymer Nanostructures for Switchable Bioelectrocatalysis

Fengjin Qu[1,2,3,4], Xiaoyan Ma*[,2], Julien E. Gautrot*[,3,4]

[1]*Center for Regenerative and Reconstructive Medicine, Med-X Institute, the First Affiliated Hospital of Xi'an Jiaotong University, Xi'an 710061, China*

[2]*Department of Applied Chemistry, School of Natural and Applied Sciences, Northwestern Polytechnical University, Xi'an 710072, China*

[3]*Institute of Bioengineering and* [4]*School of Engineering and Materials Science, Queen Mary University of London, Mile End Road, London E1 4NS, U.K.*

*To whom correspondence should be addressed: m_xiao_yana@nwpu.edu.cn, Department of Applied Chemistry, School of Natural and Applied Sciences, Northwestern Polytechnical University, Xi'an 710072, China; j.gautrot@qmul.ac.uk, Institute of Bioengineering and School of Engineering and Materials Science, Queen Mary University of London, Mile End Road, London E1 4NS, U.K.

Highlights:

- PNIPAM brushes can be re-initiated from enzyme-modified PDMAEMA brushes to generate block-copolymer brush architectures with precisely positioned biocatalysts.
- Block copolymer brush nanoarchitectures (grafting density, thickness and crosslinking) significantly impact the responsiveness of the interface and stable enzyme embedding.
- Controlling the block copolymer nanoarchitecture modulates sensing of analytes such as glucose by precisely embedded biocatalytic sites.
- Polymer brush nanoarchitectures with precisely positioned biocatalytic sites enable the development of stable switchable bioelectrocatalytic sensors whilst retaining excellent sensitivity, dynamic range and reversibility upon cyclic switching, a combination of features and properties that had not been achieved in previous switchable biosensors.

Abstract:

The ability to reversibly switch bioelectrocatalytic sensors is attractive for the design of biomonitoring platforms displaying a complex environmental response, or for the protection of biosensors. However, the retention of reversible biocatalytic properties upon multiple environmental cycles, with broad detection range, low signal-to-noise and limit of detection remains challenging. In this report, we demonstrate the precise positioning of the enzyme glucose oxydase within block-copolymer brush nanostructures, via the re-initiation of N-isopropylacrylamide (NIPAM) polymerisation from enzyme-decorated poly(dimethylaminoethyl methacrylate) (PDMAEMA) blocks. We find that the precise design of polymer brush grafting density, thickness and

crosslinking of the PNIPAM block enables the stable positioning of biocatalytic sites close to electrode surfaces. The control of the polymer brush nanostructure, its conformation and the distribution of biocatalytic sites is characterised via a combination of in situ ellipsometry, X-ray photoelectron spectroscopy, grazing angle FTIR and surface plasmon resonance. In turn, cyclic voltammetry and electrochemical impedance spectroscopy demonstrate that such control of the polymeric nanostructures confers a unique combination of low limit of detection (23.9 μM), a broad dynamic range of glucose sensing (0.05 to 12.8 mM) and true "OFF" state upon pH or thermal stimulation, whilst retaining excellent performance over repeated switching cycles of the sensor. Therefore, hierarchical biocatalytic polymer brushes display unique properties for the design of responsive biosensors and complex multi-functional gating platforms.

Keywords: bioelectronics, stimuli-responsive polymer, polymer brush, surface-initiated ATRP, enzymatic catalysis

1. Introduction

"Switch-on-demand" bioelectrocatalytic systems are integral elements for the construction of "smart" bioelectronic devices (e.g., biosensors, biofuel cells), biocomputing systems and drug release devices with self-diagnosis capability (Gamella et al., 2014; Katz and Willner, 2003; Privman et al., 2009; Wang et al., 2018). Switchable bioelectrocatalysis is typically triggered by external stimuli mediated by stimuli-responsive materials functionalising the surface of electrodes. For example, changes in structural and physical properties (molecular conformation, hydrophobicity/hydrophilicity balance, charge density) of stimuli-responsive polymers can modulate electron transfer and mass transport at electrodes (Qu et al., 2017; Zang et al., 2018). This results in reversible switching between "active" and "inactive" states for specific (bio)electrocatalytic reactions at electrodes.

The response of bioelectrocatalysis to physiological or biochemical stimuli constitutes an advantage for biosensing and biomonitoring. A variety of responsive polymers have been developed, for example based on self-assembled monolayers, thin films or assemblies of nano/microparticles (Chen et al., 2019b; Schmidt et al., 2008; Zakharchenko et al., 2018; Zhang et al., 2017). The physico-chemistry of polymer interfaces, their architecture and aggregation resulted in widely differing behaviours. For example, bioelectrodes functionalised with thermosensitive poly(N-isopropylacrylamide) (PNIPAM) and its copolymers display an "OFF" state at

temperatures above its lower critical solution temperature (LCST) and switch the interface "ON" below the LCST (Parlak et al., 2015a; Wang et al., 2015; Yu et al., 2016). However, other studies presented an opposite switching behaviour (Akkaya et al., 2018; Liang et al., 2017; Mishra et al., 2017), depending on affinity and diffusion of electrolytes within thermosresponsive brushes, their association with comonomers and the occurrence of complex phase transitions (Bokias et al., 2000; Garcia et al., 2012).

In addition to such complex responsive behaviour, other hurdles need to be overcome to improve the efficiency and sensitivity of biocatalytic and biosensing platforms. For example, intelligent polymers and hydrogels typically exhibit poor conductivity. Therefore their effect on electron transfer and molecular diffusion in the "active" state should be carefully engineered. The diffusion of reactants and wettability of polymeric interfaces therefore appear important parameters for the design of bioelectrocatalytic systems (Liang et al., 2017; Zhou et al., 2007). Although polymeric coatings with low density and heterogenous coverage might be beneficial for charge transfer and mass diffusion to electrodes, their disordered and sparse polymer structure limits the switching behaviour and does not allow a tight control of electrochemical reactions at corresponding interfaces (Akkaya et al., 2018; Garcia et al., 2012; Parlak et al., 2015b). Thus, it is crucial to balance the electrochemical performance and switching behaviour. Last but not least, the introduction of enzymes or redox proteins at corresponding interfaces requires to retain the catalytic activity and affinity to specific analytes (Rosenthal et al., 2018). Overall, the structure and architecture of responsive polymer

coatings are key factors to precisely control switchable bioelectrochemical processes at bioelectrodes.

Diverse strategies have been developed for the construction of responsive biocatalytic interfaces. A simple drop-casting method can be applied for the physisorption of polymers and enzymes on electrode surfaces (Akkaya et al., 2018; Chen et al., 2019a; Mishra et al., 2017; Parlak et al., 2015a; Zhang et al., 2012). Switchable bioelectrodes can also be assembled by using radical polymerisation or electropolymerisation in precursor solutions (Chen et al., 2015; Karbarz et al., 2009; Wang et al., 2015; Yu et al., 2016). However, the engineering of interfaces using such polymer coatings and the electrochemical responsiveness of corresponding bioelectrodes remains difficult to control. In particular, a high residual electrocatalytic current in the "OFF" state is typically observed, and the biocatalytic properties of interfaces significantly decrease upon repeated environmental cycling (e.g. of temperature or pH) (Liu and Hu, 2011; Liu et al., 2010; Parlak et al., 2015b; Yao et al., 2014). To a large extent, such behaviour is proposed to arise from the difficulty to precisely control the positioning of biocatalytic sites within the polymer coating. These factors will limit the range of physico-chemical properties achieved and the application of the modified bioelectrodes. The preparation of polymer brushes via controlled surface-initiated polymerisation allows the sophisticated design and independent control of polymer architecture and chemistry on various solid surfaces (Krishnamoorthy et al., 2014; Zoppe et al., 2017). It also allows the systematic study of

the impact of physicochemical parameters of polymer brushes on switching behaviour, electrochemical performance and the loading of enzymes at electrodes. Optimised polymer brushes can potentially control electron and mass transport in a precise and predictable manner, suitable for the fabrication of complex multi-responsive electrochemical platforms (Garcia et al., 2012), including for nanotheranostic applications (Li et al., 2020). Although protein adsorption to polymer brushes has been relatively widely applied and studied (Krishnamoorthy et al., 2014; Wei et al., 2014), the precise control of polymer brushes for bioelectrocatalysis remains an important challenge to address. Specifically, the precise positioning of enzymes within polymer brush architectures with high grafting densities has not yet been achieved, due to the difficulty to control protein infiltration within dense polymer brushes. Such control will enable the fine tuning of responsive and biocatalytic properties with greater sensitivity, independently.

To address this issue, we propose to exploit the ability to re-initiate the growth of polymer brushes in order to generate block copolymer structures. We report that such re-initiation is possible even after enzyme immobilisation, therefore enabling to control the positioning of biocatalytic sites with unprecedented control within dense polymer brush coatings. This strategy enabled us to develop dual-switchable enzymatic bioelectrodes with defined architectures for reversible switching and sufficient enzyme loading. pH-responsive poly(dimethylaminoethyl methacrylate) (PDMAEMA) brushes with varying grafting densities and thicknesses were first grown from the gold

electrodes via surface-initiated atom transfer radical polymerisation (SI-ATRP) (Scheme 1). We introduced glucose oxidase (GOx) within the resulting brushes prior to re-initiation and growth of PNIPAM blocks, therefore resulting in the integration of enzymatic sites in well-defined location within dense thermoresponsive polymer brushes. X-ray photoelectron spectroscopy, surface plasma resonance and *in situ* ellipsometry are used to investigate the morphology and detailed architecture of the resulting hierarchical biocatalytic brushes. We then systematically investigated the relationship between the architecture of the resulting block copolymer brushes and the responsive biocatalytic performance of the resulting biosensors. These bioelectrodes exhibited sensitive electrocatalytic activity towards glucose oxidation and stable reversible switching. Hence this work demonstrates the proof of concept of precise positioning of biocatalytic sites in hierarchical polymer brushes for the design of switchable biosensors and biocatalytic systems.

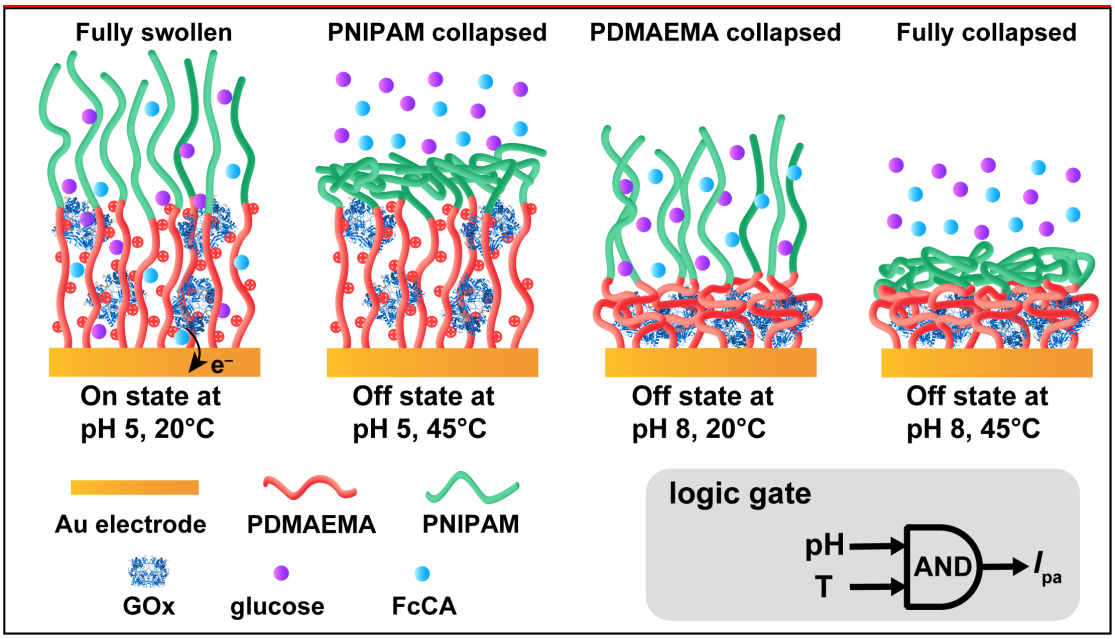

Scheme 1. Schematic illustration of Au–PDMAEMA/GOx–b–PNIPAM electrodes and their responsiveness to pH and temperature. The inset presents the type of logic gate associated with such dual-responsive interfaces.

2. Experimental

Details of reagents and materials and supplementary methods for the fabrication of sensors and their characterisation can be found in the supplementary information.

2.1 Fabrication of Switchable Bioelectrodes

2.1.1 Synthesis of PDMAEMA Brushes

A solution of $CuBr_2$ (18 mg, 80 μmol), bipy (320 mg, 2.05 mmol), and DMAEMA (6.6 g, 42 mmol) in water/ethanol (4:1, *v*/*v*; 30 mL) was degassed using argon bubbling for 30 min. CuCl (82 mg, 828 μmol) was then added to this solution quickly, and the resulting mixture was sonicated to ensure full dissolution of CuCl and further degassed for 30 min before polymerization. Initiator-coated electrodes were placed in reaction

vessels and degassed via four cycles of vacuum/nitrogen. Subsequently, 1 mL of DMAEMA solution was transferred to reaction vessels under an inert atmosphere via a syringe. The polymerization was stopped by immersing the coated gold electrodes in ultrapure water followed by washing with copious amounts of ethanol and drying under a nitrogen stream.

2.1.2 Adsorption of GOx to PDMAEMA Brushes

As the isoelectric point of GOx is around 4.2 (Wilson and Turner, 1992), it can readily adsorb within positively charged PDMAEMA brushes (p*K*a = ~7.0) via electrostatic interaction, at pH 5. Thus, PDMAEMA brushes were soaked in GOx solutions (pH 5) with a range of concentrations (0.5, 1, 5, 10 mg mL^{-1}) in for 30 min, and rinsed with ultrapure water.

2.1.3 Growth of PNIPAM Layer on GOx/PDMAEMA Brushes

PNIPAM brush growth was reinitiated from the freshly prepared (GOx/)PDMAEMA brushes via ATRP. A solution of $CuBr_2$ (18 mg, 80 μmol), bipy (320 mg, 2.05 mmol), NIPAM (4.752 g, 42 mmol) and BIS (0–0.462 g, 0–3 mmol) in pure water (30 mL) was prepared, followed by the same process for synthesis of PDMAEMA brushes. After polymerisation, since Cu(II) ions adsorbed onto the active centre of GOx and resulted in the decline of its enzymatic activity, the enzymatic electrode were soaked in 1 mM EDTA solution for 10 min, followed by washing with copious amounts of ultrapure water. The as-prepared diblock copolymer brushes-coated enzymatic electrodes were

stored in PBS (pH adjusted to 5.0) at 4°C until used.

2.2 Characterisation

2.2.1 Ellipsometry Measurements

Ellipsometry measurements were carried out with an *α*-SE instrument from J. A. Woollam at an incidence angle of 70° (multi-wavelength within the range of 380-900 nm). For dry samples, a simple gold substrate/Cauchy film model was used. For wet samples, substrates were placed in an in-house-built chamber fitted with quartz windows normal to the laser beam path. Measurements were carried out in triplicate. The swelling and collapse of brushes in different conditions were studied via *in situ* ellipsometry. Swelling ratios are given as swollen height/dry height. It is worth noting that we only refer to the values of dry thickness of brushes in this work to prevent confusion, unless otherwise stated in the text.

2.2.2 Surface Plasmon Resonance (SPR)

SPR was used to quantify interactions between GOx and polymer brushes with a Biacore 3000. SPR chips were coated with polymer brushes prior to mounting on a substrate holder. Mounted chips were docked, primed with the running buffer (PBS) for 3 min, and equilibrated at 10 μL min^{-1} flow rate until a stable baseline was obtained. Then, 50 μL of GOx solutions was injected at 1 mg mL^{-1}. After injection, washing with running buffer was continued at a 10 μL min^{-1} flow rate. The enzyme adsorption level

was measured after 1200 s. GOx adsorption studies via SPR were carried out with chips coated by PDMAEMA, PNIPAM and block copolymer brushes with various thicknesses at different grafting densities. All measurements were carried out in triplicate (three separate chips freshly prepared).

2.2.3 X-ray Photoelectron Spectroscopy (XPS)

XPS analysis was measured on the Kratos AXIS ULTRA^{DLD} electron spectrometer with Al Kα X-ray source (1486.6 eV) operated at 150 W. A pass energy of 160 eV and a step size of 1 eV were used for survey spectra. For high energy resolution spectra of regions, a pass energy of 20 eV and a step size of 0.1 eV were used. Sample charging effects were eliminated by correcting the observed spectra with the C 1s BE value of 285.0 eV.

2.2.4 Electrochemical Experiments

Cyclic voltammetry (CV) at electrodes was performed on an Autolab PGSTAT30 potentiostat (Metrohm) with a conventional three-electrode cell compromised of a gold electrode as a working electrode, a platinum wire as a counter electrode and an Ag/AgCl (Sat. KCl) as reference electrode. Electrochemical impedance spectroscopy (EIS) was measured in solutions of 5 mM $K_3Fe(CN)_6/K_4Fe(CN)_6$ (1:1) and 0.1 M KCl within the frequency range of 0.01 Hz to 10 kHz. Differential pulse voltammetry (DPV) was performed with modulation amplitude of 25 mV, modulation time of 50 ms and step potential of 5 mV.

For environmental cycling (and responsiveness) assays, electrodes were first immersed into a pH 5.0 solution at 20°C for 1 min, followed by CV measurements with multiple cycles until a stable CV trace was acquired. The medium was then heated to 45°C and CV measurements were repeated. The electrode was removed from the pH 5.0 medium, rinsed with deionised water and placed into a pH 8.0 medium at 20°C, followed by the same procedure as in pH 5.0 medium. The process was repeated as indicated in Fig. 5 (6 cycles, 24 changes in pH and temperature). All cycles for one given experiment were recorded on the same electrode/sensor.

2.2.5 Statistical Analysis

Data are reported as means ± standard deviation for groups of at least three replicates. An unpaired two-tailed Student's t test was used for assessing statistical significance (*$p < 0.05$, **$p < 0.01$, ***$p < 0.001$).

3. Results and Discussion

3.1 Adsorption of Enzymes to PDMAEMA, PNIPAM and Diblock Copolymer Brushes

The formation of PDMAEMA brushes with controlled density at the surface of gold electrodes was first investigated, demonstrating excellent control of thickness and brush density (see Supplementary Results and Discussion S2.1, Figures S1-S2 and Table S1). The interaction of GOx with different polymer brushes was then quantified SPR and

ellipsometry (see Supplementary Results and Discussion S2.2, Figures 1 and S3-S4). We studied the GOx adsorption into PDMAEMA brushes with varying grafting densities. Upon exposure to GOx solutions, the adsorbed mass rapidly increased and reached a plateau within 300 s, depending on grafting density, indicating the infiltration and sequestration of negatively charged GOx within cationic brushes (Figure 1A), similarly to what was observed for other biomacromolecules (Krishnamoorthy et al., 2017; Qu et al., 2019). At low brush densities (0.21 chains nm^{-2}), the stability of infiltration reduced. The adsorption level of GOx was maximized at intermediate brush grafting density (Figure 1B), reaching a maximum (2,600 ng cm^{-2}) at 0.33 chains nm^{-2} for 15 nm PDMAEMA brushes. This was confirmed by ellipsometry (Figure S5). Molecule diffusion within polymer brush restricts adsorption and is modulated by molecular size, conformational freedom, brush grafting density and chain length (Krishnamoorthy et al., 2017; Qu et al., 2019). Experimental and theoretical work had previously identified that, for molecular diffusion to occur within polymer brushes (in the case of weakly interacting molecules and brushes), the radius of gyration of molecules should be small compared to the dimensions of the brush. The maximum GOx adsorption observed at intermediate grafting densities is therefore proposed to reflect the enhanced infiltration of GOx (with an average diameter of 8 nm and an axial ratio of 2.5:1 (Wilson and Turner, 1992)) within brushes.

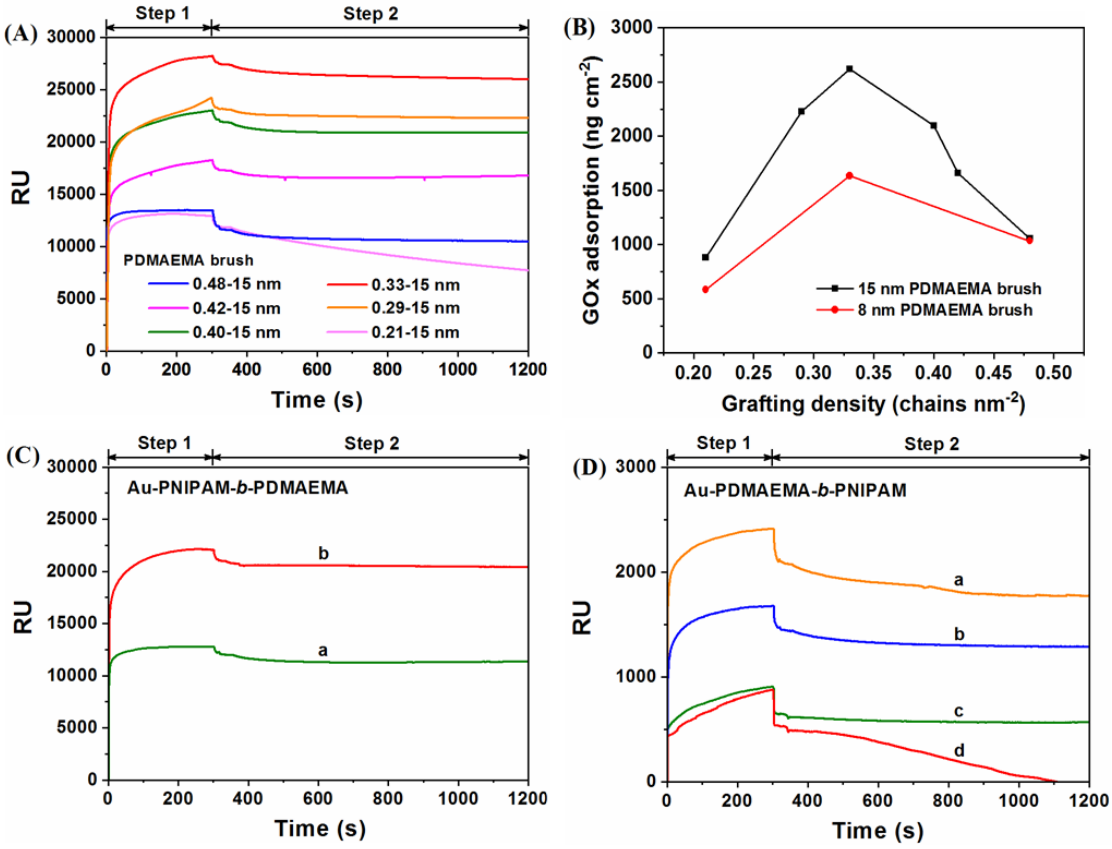

Figure 1. Adsorption of GOx (1 mg mL^{-1}) to PDMAEMA brushes monitored by SPR. (A) SPR traces recorded for 15 nm PDMAEMA brushes at grafting densities of 0.48, 0.42, 0.40, 0.33, 0.29 and 0.21 chains nm^{-2}. (B) Summary of binding levels measured for GOx on 8 and 15 nm PDMAEMA brushes, after 900s of washing with running buffer as a function of grafting density. SPR traces on (C) Au–PNIPAM–*b*–PDMAEMA with 15 nm PNIPAM and (a) 8 nm, (b) 15 nm PDMAEMA. SPR traces on (D) Au–PDMAEMA–*b*–PNIPAM with 15 nm PDMAEMA and (a) 8 nm, (b) 15 nm linear PNIPAM brush, (c) 8 nm, (d) 15 nm cross-linked PNIPAM (33 mM of BIS). Step 1: exposure to GOx solution in the running buffer (PBS). Step 2: exposure to the running buffer.

The impact of PDMAEMA brush dry thickness on GOx adsorption was found to depend on the brush grafting density (Figure 1B). For dense brushes (100% initiator; 0.48 chains nm^{-2}), GOx adsorption was insensitive to the brush dry thickness (Figure S5-S6). This suggested that GOx macromolecules poorly infiltrated dense PDMAEMA brushes, resulting in adsorption restricted at the brush–solution interface. In contrast, at

lower grafting densities, the adsorption of GOx was regulated by the brush thickness and associated surface density of cationic moieties. For example, for 0.33 chains nm^{-2} PDMAEMA brushes, GOx adsorption levels increased with the brush dry thickness.

We next investigated the interactions between GOx and PNIPAM brushes at 20°C and 45°C (Figure S7). Upon exposure to GOx solutions at 20°C, an initial adsorption occurred on PNIPAM brushes to a relatively low level (57 ng cm^{-2}), followed by a rapid desorption upon washing the brush surface with running buffer. The rapid and low magnitude transient adsorption observed is likely the combined result of mismatch in the refractive index of the buffer as well as weak and reversible adsorption. This is consistent with the protein-resistance of hydrophilic PNIPAM below its LCST (Xue et al., 2011). Above its LCST, a slightly higher level of binding was observed, although remaining below 115 ng cm^{-2}, in particular at lower grafting densities.

We next examined the adsorption of GOx to block-copolymer brushes (Figure 1C and 1D). In the case of PDMAEMA outer blocks (designated as Au–PNIPAM–*b*–PDMAEMA), GOx adsorption was comparable to that observed to homopolymer PDMAEMA brushes. When the protein-resistant PNIPAM was generated as the outer block (Au–PDMAEMA–*b*–PNIPAM), GOx adsorption was significantly reduced, in agreement with the restricted diffusion to the cationic block. GOx adsorption was further reduced by increasing the thickness of PNIPAM brush and its crosslinking with a difunctional monomer. Hence simple adsorption of GOx to the lower block of a PDMAEMA–*b*–PNIPAM brush appeared to be unsuitable for the design of responsive

electrobiocatalytic systems, due to the lack of significant diffusion of GOx through the brush nanostructure. In addition, although GOx adsorption was strong to Au–PNIPAM–*b*–PDMAEMA brushes, the distance of adsorbed GOx was expected to be intrinsically limiting for electron transfer to corresponding electrodes.

3.2 Fabrication and Characterisation of Diblock Copolymer Brushes with Precisely Positioned Enzyme

To allow the precise positioning of enzymes within the block-copolymer nanostructures, we proposed to adsorb GOx onto PDMAEMA brushes prior to the growth of PNIPAM outer blocks. This architecture was designed to ensure the proximity of GOx from the electrode surface, to promote rapid and localised diffusion of electroactive species, whilst positioning PNIPAM brushes ideally to limit mass transfer to the biocatalytic site. The resulting brushes are designated Au–PDMAEMA/GOx–*b*–PNIPAM. We first investigated the reinitiation kinetics of PNIPAM from PDMAEMA brushes via ellipsometry, with and without GOx adsorption. To accelerate the growth rate of PNIPAM blocks and reduce the risk of denaturation of the enzyme, polymerisations were carried out in deionised water. The growth of PNIPAM from PDMAEMA chains grafted at a density of 0.33 chains nm^{-2} remained well-controlled even after adsorption of GOx (Figure S8A). The outer block growth rate decreased sharply with increasing PDMAEMA grafting densities (Figure S8B) and increasing GOx concentration on PDMAEMA brush. Therefore, the aggregation of

GOx at the surface of PDMAEMA inner blocks shielded polymer end chains from re-initiation, a phenomenon that was more pronounced at higher grafting density, for which GOx infiltration was restricted and adsorption was confined to the brush-solution interface. Overall, PDMAEMA brushes with a thickness of 15 nm and grafting density of 0.33 chains nm^{-2} were selected for further PNIPAM growth and biocatalytic evaluation.

The hierarchical structure of enzyme-embedded copolymer brushes was confirmed by XPS and grazing angle Fourier transform infrared spectroscopy (grazing angle FTIR) (Figures S9 and S10 and Supplementary Discussion S2.4). XPS confirmed that, after PNIPAM growth, the C_{1s} spectrum of resulting surfaces was almost identical to that of a single homopolymer PNIPAM brush, fitted with three peaks at 284.5, 285.9 and 287.1 eV, assigned to C─C/C─H, C─N and N─C═O groups, respectively, in agreement with the limited depth probed by XPS (5-10 nm) and the comparatively thick PNIPAM outer block characterised (15 nm) (Figure S9E and F). In contrast, after re-initiation of PNIPAM from GOx-adsorbed PDMAEMA brushes, the IR spectrum exhibited the characteristic peaks of PDMAEMA, GOx and PNIPAM, in agreement with grazing angle FTIR probing the entire depth of the coating.

3.3 pH-/Thermo-Sensitive Property of Block Copolymer Brushes

The pH- and thermo-sensitive properties of PDMAEMA and PNIPAM homo- and block-copolymer brushes were next explored via *in situ* ellipsometry. The surface

wettability of polymer brush-decorated substrates at different temperatures and pH was also characterised via water contact goniometry. At pH 5.0, the PDMAEMA brushes were hydrophilic (contact angles of ~10°) and swollen, due to the protonation of tertiary amine groups (Figure S11A and B). The brush swelling ratio at pH 5.0 ranged from 2.8 to 4.7, depending on the grafting density, whereas brush swelling moderately decreased, from 3.9 to 3.6, as the brush thickness increased (for a density of 0.33 chains/nm^2). This is due to the increased length of individual polymer chains required to generate sparse brushes displaying identical dry thicknesses, leading to increased swelling ratios. Upon switching to pH 8.0, polymer chains were deprotonated. Polymer brushes became relatively hydrophobic (contact angle near 60°) and collapsed back to their dry thickness, except for the thicker brushes (30 nm), which presented only partially collapsed structures (but we confirmed that they fully collapsed when dried again). This indicates that the collapse of thick brushes is not homogeneous in solution, possibly resulting in a hydrophobic shell in the upper brush compartment that prevents further diffusion of water molecules and protons. Such phenomenon had previously been reported for other thermo-responsive brushes (Laloyaux et al., 2010).

The thermo-responsive PNIPAM has a LCST at 32°C in bulk solution, a phase transition that seems to decrease slightly to around 28°C for polymer brushes, depending on grafting density (Ishida and Biggs, 2010). As a result, at 20°C, PNIPAM chains were relatively hydrophilic (contact angle above 30°) and swell to ratios lower than those observed for PDMAEMA brushes, due to the neutral character of the former

brushes (Figure S11C and D). When the solution and surface were heated to 45°C, PNIPAM chains were dehydrated and collapsed, with contact angles in the range of 50–70°. When brushes were crosslinked, as the concentration of BIS crosslinker increased, the brush swelling reduced slightly, due to the conformational restriction imposed by crosslinks. In parallel, the hydrophobicity of PNIPAM brushes (at a grafting density of 0.33 chains nm^{-2}) increased with crosslinking, both below and above the LCST.

As expected, block copolymer brushes exhibited dual-responsiveness to pH and temperature, evidenced by water contact goniometry and ellipsometry (Figure 2A and B). When either the temperature increased to 45°C or the pH to 8.0, corresponding responsive blocks collapsed, resulting in a partial decrease of the overall brush thickness. As for homopolymer brushes, swelling ratios decreased as the brush thickness increased. In addition, the collapse of the inner layer was found to be only partial, perhaps highlighting that the local composition of this block and its confinement and restricted conformation altered its responsive behaviour. This is consistent with the behaviours reported in the literature (Plunkett et al., 2006). Loading GOx in the PDMAEMA compartment (prior to re-initiation with PNIPAM or after growth of an outer PDMAEMA block) had a negligible impact on this responsive behaviour (Figure 2C and D). The dry thickness of Au–PNIPAM–*b*–PDMAEMA/GOx reduced gradually in following switching cycles, due to desorption of GOx from the outer PDMAEMA blocks, after collapse at high pH, whereas the dry thickness of Au–PDMAEMA/GOx–*b*–PNIPAM remained steady.

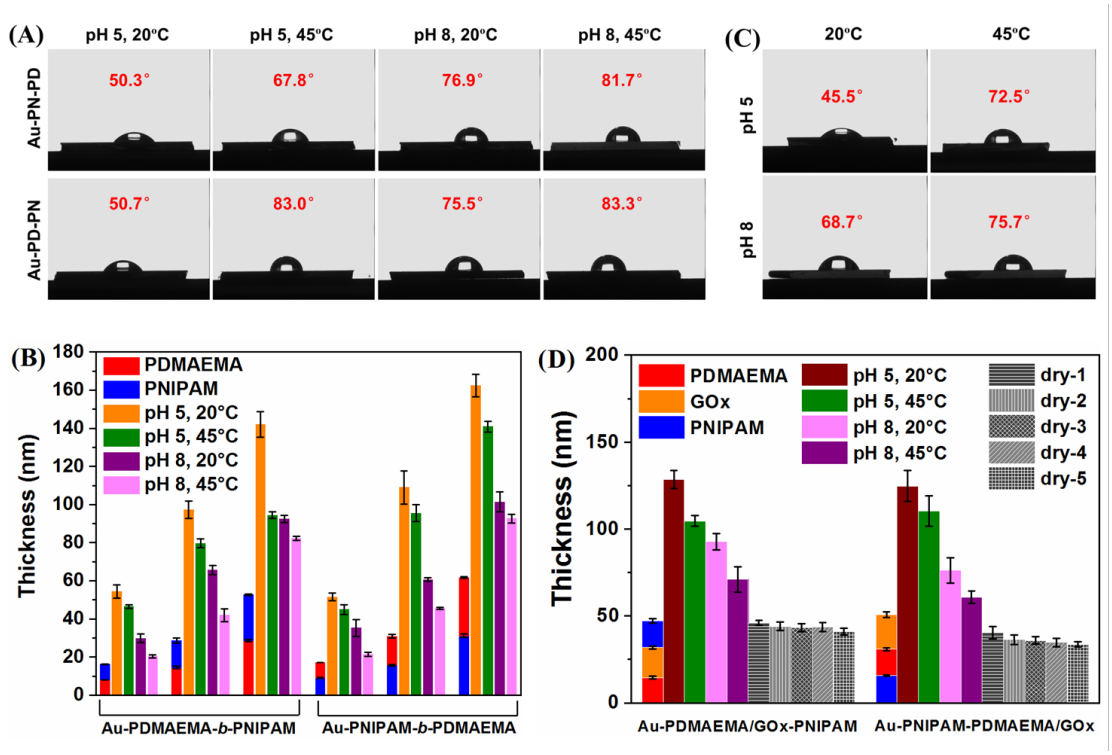

Figure 2. Static water contact angle images of (A) Au–PNIPAM–*b*–PDMAEMA (Au–PN–PD for short in this figure) and Au–PDMAEMA–*b*–PNIPAM (Au–PD–PN for short in this figure) substrates, (C) Au–PDMAEMA/GOx–*b*–PNIPAM substrates at a grafting density of 0.33 chains nm^{-2} with a dry thickness of 15 nm for each block, at pH 5 and 20ºC, pH 5 and 45ºC, pH 8 and 20ºC, pH 8 and 45ºC. Evolution of the ellipsometric thickness of (B) copolymer brushes and (D) enzyme-loaded copolymer brushes, at a grafting density of 0.33 chains nm^{-2} with a dry thickness of 15 nm for each block, on gold wafers in dry conditions and in different aqueous solutions. (Grey columns are the dry thicknesses of enzyme-loaded polymer brushes after repetitive washing with deionised water; the number of washes is indicated).

Cyclic voltammograms of different electrochemical probes were carried out at different pH and temperatures, to demonstrate the controlled switching mechanism of bio-electrochemical properties at block-copolymer modified electrodes (Figure S12). The effects of pH and temperature on CV response in the presence of $[Fe(CN)_6]^{3-/4-}$, $[Ru(NH_3)_6]^{2+/3+}$ and ferrocenecarboxylic acid (FcCA) probes followed similar trends. At low pH (5.0) and temperature (20°C), both PDMAEMA and PNIPAM blocks are

hydrated and swollen, leading to effective probe diffusion and enabling electron transfer to the electrode. In contrast, PDMAEMA and/or PNIPAM collapsed at pH > 8.0 and/or 45°C, which blocked the diffusion of probes to the electrode surface and reduced the current intensity of redox peaks of corresponding probes in CV traces. It is worth noting that the redox peak current displayed no obvious difference at bare electrode upon changing the pH and temperature conditions (Figure S13). Since $[Fe(CN)_6]^{3-/4-}$, $[Ru(NH_3)_6]^{2+/3+}$ and FcCA carry different charges, these results demonstrated that it is the phase transition and associated change in block morphology that is dominating the electrochemical switching of the electrode, rather than changes in surface charge of polymer brushes (for example modulating sequestration of oppositely charged or hydrophobic probes).

3.4 Impact of Responsiveness of PDMAEMA Brushes

The impact of the polymer brush architecture on the electrochemical behaviour was investigated next, with FcCA as probe. The effect of the brush grafting density on the electrochemical responsiveness of the corresponding electrode was examined (Figure 3 and S14). On dense PDMAEMA brushes, an asymmetrical shape of the FcCA reduction peak was observed at pH 5.0, indicating the irreversibility of the electrochemical reaction, presumably due to the strongly positive electrostatic potential of the surface resulting in the rapid ejection of oxidised species (Figure 3A). Compared to bare gold electrodes (shown in Figure S13), dense PDMAEMA brush-grafted

electrodes displayed reduced peak currents and increased peak potential separation (ΔE_p), further suggesting that the dense and insulating polymer brush suppressed the electrochemical reaction of electroactive probes. This effect was gradually reduced at lower brush densities. With increasing polymer brush thicknesses, the peak currents decreased while ΔE_p increased, particularly on dense polymer brushes, due to the more restricted diffusion of electroactive probes and associated electron transfer (Figure S15). In all cases, upon switching the pH of the medium to 8.0, the redox peak currents were reduced dramatically, as the diffusion of electroactive probes and charge transfer were severely restricted by the collapsed and hydrophobic PDMAEMA brushes. By decreasing the brush grafting density, the collapsed polymer chains could not fully cover the electrode surface and block redox processes, leading to an increase in peak current at pH 8.0. Overall, thick dense polymer brushes resulted in the blocking of electrochemical reactions at high pH, but lower-density brushes with short chain length (8 nm, 0.33 chains nm^{-2} brush) were unable to act as efficient barriers and presumably did not fully cover the electrode surface.

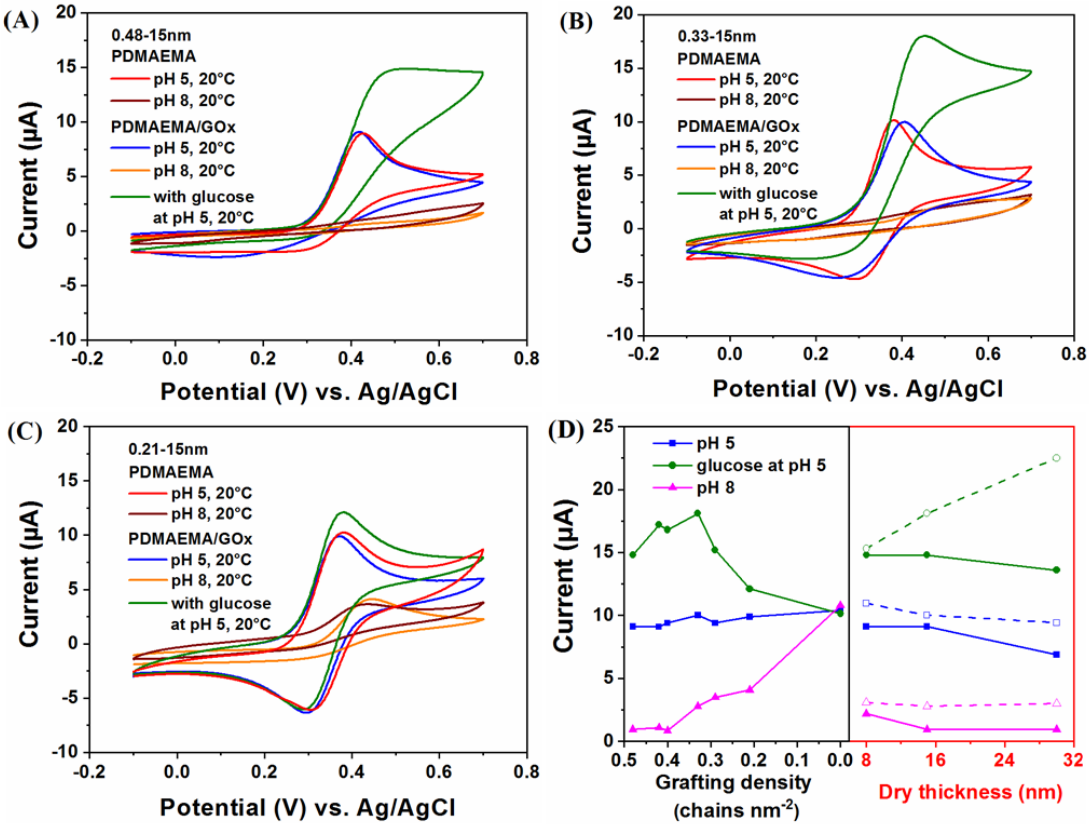

Figure 3. CVs of Au–PDMAEMA and Au–PDMAEMA/GOx at grafting densities of (A) 0.48, (B) 0.33 and (C) 0.21 chains nm^{-2} with a dry brush thickness of 15 nm. Cycling was carried out in PBS containing 1 mM FcCA at pH 5, pH 8, or in the presence of 10 mM glucose at pH 5. Data were recorded at 20ºC. Scan rate: 50 mV s^{-1}. (D) Dependence of oxidation peak current of FcCA at Au–PDMAEMA/GOx electrode as a function of (left) grafting density with 15 nm brush thickness, and (right) dry thickness at a grafting density of 0.48 (solid line) and 0.33 chains nm^{-2} (dash line). Note that a grafting density of 0.0 chain/nm^2 corresponds to bare gold substrates.

3.5 Dual-Switchable Bioelectrocatalysis at Hierarchically-Structured Modified Electrodes

The entrapment of GOx within the PDMAEMA brush had a negligible impact on probe electrochemistry (FcCA) at corresponding interfaces. However, with the addition of glucose in the electrolyte solution, a large oxidation peak was observed at GOx-

loaded PDMAEMA brush electrodes, at low pH (Figure 3). This behaviour is a typical signature of the electrochemical oxidation of glucose to gluconolactone catalysed by GOx mediated by FcCA in solution (Cass et al., 1984). This oxidation peak current (I_{pa}) was dependent on the activity of embedded enzymes, molecular diffusion and charge transfer at electrode. At reducing brush grafting density (0.33 chains nm^{-2}), an increasing I_{pa} and decreasing over-potential were observed, which can be attributed to the synergistic impact of improved enzyme loading and molecular diffusion. However, the I_{pa} decreased clearly with electrodes functionalised with lower grafting-density PDMAEMA brushes, due to the reduced GOx loading (Figure 1A). Similarly, with increasing polymer brush thicknesses, the I_{pa} decreased for dense polymer brushes (see Figure S15), as a result of the restricted molecular diffusion and greater distance of GOx from the surface (SPR had shown that the amount of GOx did not vary; Figure S6). In contrast, on PDMAEMA brushes with intermediate grafting densities and increasing thickness (30 nm), a sharp increase of I_{pa} in the presence of glucose was observed (Figure S15), which was ascribed to the dramatically enhanced GOx adsorption on thicker polymer brushes (see corresponding SPR in Figure S6).

We next investigated the impact of the PNIPAM outer block architecture on the switching of electrochemical processes at corresponding electrodes (Figure 4). With increasing thicknesses of PNIPAM blocks, the FcCA oxidation peak current could be significantly restricted, but was not completely suppressed by the collapsed PNIPAM block at pH 5.0 and 45°C (see Supplementary Results and Discussion S2.3, Figure 4A

and S16). With increasing levels of crosslinking (%BIS), a gradual reduction in the peak current associated with FcCA oxidation observed in the presence of glucose was observed, indicating a restriction in molecular diffusion through the crosslinked shell. Thus, a crosslinker concentration of 33 mM BIS within the PNIPAM block was used to confer a balance between the restriction of outer block dewetting upon hydrophobic collapse and sufficient molecular diffusion in the swollen state. With increasing PNIPAM outer block thicknesses, the peak current decreased slightly and the I_{pa} in the presence of glucose decreased similarly, at pH 5.0 and 20°C. This is likely due to the restricted diffusion of electroactive species by the PNIPAM outer block. When the pH 5.0 electrolyte solution was heated to 45°C, PNIPAM chains collapsed, hindering the diffusion of electroactive FcCA and blocking the electron transfer processes at the electrode surface. The extent of this effect was improved with increasing PNIPAM block length. In contrast, at higher temperature, the CV peak current of FcCA at bare electrodes and PDMAEMA-modified electrodes increased. In the absence of crosslinker, despite the clear collapse of the PNIPAM outer block, molecular diffusion was not completely restricted and a clear oxidation peak was observed at high temperature (45°C; Figure 4A). To prevent the collapse of brushes into domains forming non-continuous phases, we introduced crosslinks within the outer block that aimed to enable collapse without leading to dewetting of the surface and exposure of positively charged PDMAEMA inner blocks (as was observed in other systems (Minko, 2006)).

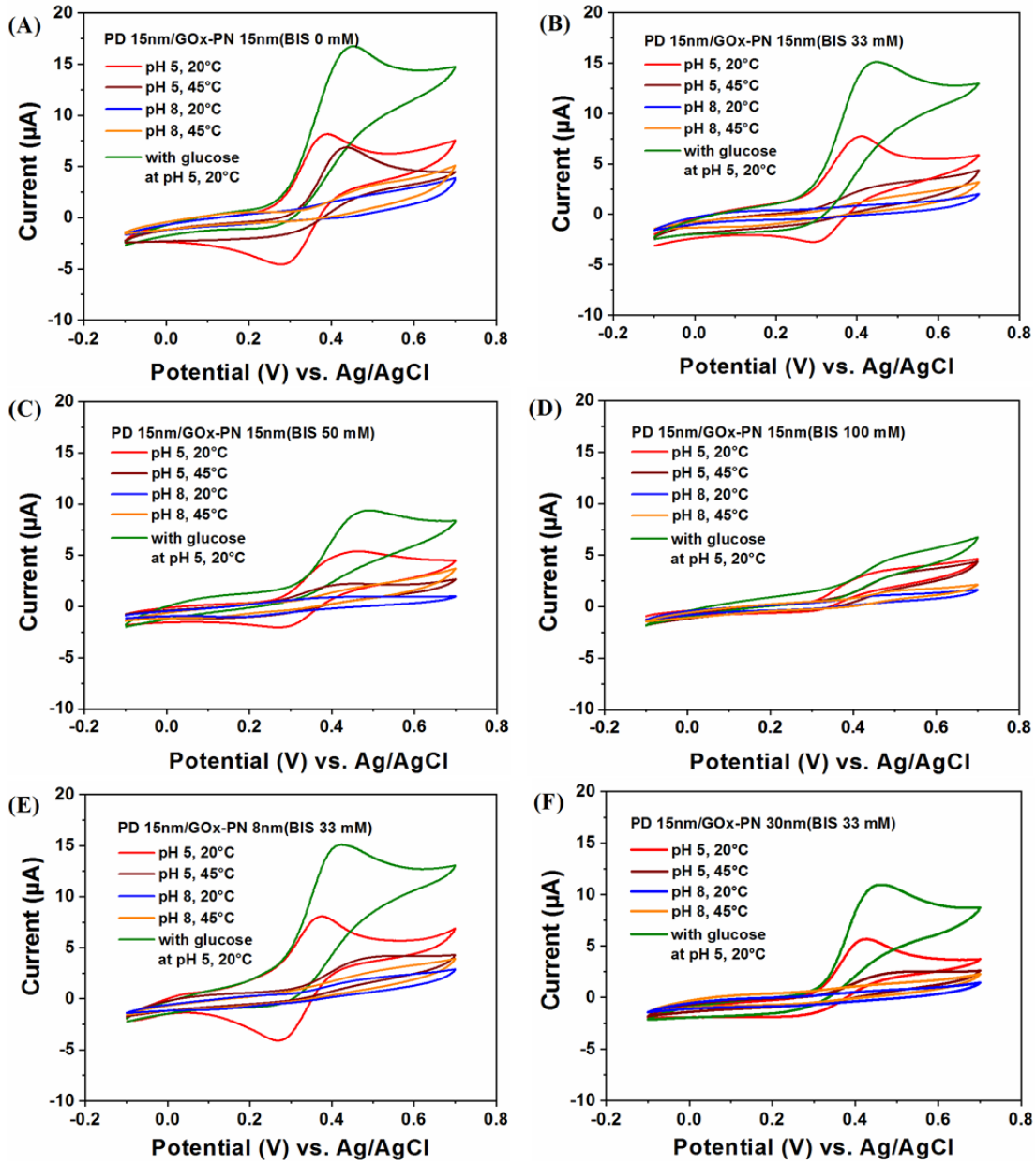

Figure 4. CVs of Au–PDMAEMA/GOx–*b*–PNIPAM (PD/GOx–PN for short in the figure) at a grafting density of 0.33 chains nm^{-2} with 15 nm PDMAEMA and cross-linked PNIPAM using BIS concentrations of (A) 0, (B) 33, (C) 50, and (D) 100 mM. CVs of PD/GOx–PN at a grafting density of 0.33 chains nm^{-2}, with 15 nm PDMAEMA and cross-linked PNIPAM thicknesses of (E) 8 nm and (F) 30 nm. Cycling was carried out in PBS containing 1 mM FcCA at pH 5 and 20ºC, pH 5 and 45ºC, pH 8 and 20ºC, pH 8 and 45ºC, and in the presence of 10 mM glucose at pH 5 and 20ºC. Scan rate: 50 mV s^{-1}.

There was no obvious increase of the peak current at GOx-coated electrode in the absence of any polymer or when GOx was allowed to infiltrate into PDMAEMA–*b*–

PNIPAM brushes, suggesting a lack of significant levels of active GOx adsorbed at these interfaces (Figure S17, consistent with SPR results). In contrast, the Au–PNIPAM–*b*–PDMAEMA electrode displayed a high GOx adsorption and effective electrocatalysis towards glucose (Figure 5A).

We explored the reversibility of dual switching behaviour of Au–PDMAEMA/GOx–*b*–PNIPAM and Au–PNIPAM–*b*–PDMAEMA/GOx electrodes (Figure 5B). Although an initially high oxidation peak current (>15 μA) was observed in both cases, the peak current reduced significantly in following electrochemical cycles, due to desorption of GOx from the outer PDMAEMA blocks, after hydrophobic collapse at high pH. In contrast, the I_{pa} of FcCA in the presence of glucose remained high (>85% after 5 cycles) for Au–PDMAEMA/GOx–*b*–PNIPAM electrodes (Figure 5B). The desorption of GOx from the outer block of Au–PNIPAM–*b*–PDMAEMA/GOx is in agreement with our ellipsometry data (Figure 2D) and with SPR data recorded during sequential pH switch (Figure S19). In contrast, the bound mass to the sensor was found to be stable after pH switch and the corresponding SPR signal recovered to its initial value. Therefore, these results demonstrated that the architecture of the block copolymer bio-interfaces proposed is not only essential for proper bioelectrocatalytic gating, but also for the retention of electrochemical properties upon repetitive environmental cycling.

The impedance data further confirmed the control of electron transfer and local diffusion of redox probe at electrodes in response to changes in pH and temperature. R_{ct} increased gradually (fitting results shown in Table 1) at electrodes functionalised

with PDMAEMA, GOx and PNIPAM, which was attributed to increased barrier to probe diffusion. At Au–PDMAEMA/GOx–*b*–PNIPAM electrodes, R_{ct} increased significantly at high pH and temperature (Figure S18 and summary in Table S2). Hence this architecture enables the construction of an AND gate as presented in the truth table (Table S3), in which a low pH and temperature are "1" states and control the output of a "1" state defined as an I_{pa}>5 μA in CVs.

Finally, we explored the sensing ability for this bioelectrode to glucose detection responding to biocatalytic stimuli. Differential pulse voltammetry (DPV) was performed to study switchable biosensing towards glucose at Au–PDMAEMA/GOx–*b*–PNIPAM electrodes (Figure 5C). At pH 5.0 and 20°C (defined as "ON" state), the I_{pa} of FcCA at Au–PDMAEMA/GOx–*b*–PNIPAM electrode increased linearly with increasing glucose concentrations in the range of 0.05–12.8 mM (R^2=0.97) with a sensitivity of 5.87 μA mM^{-1} cm^{-2} and lower detection limit of 23.9 μM (3N/S), demonstrating the retained bioactivity of entrapped GOx and associated electrocatalytic behaviour. In contrast, at pH 8 and/or 45°C, the electrode was turned to "OFF" state. Enzymatic catalysis was suppressed (the electrooxidation current was reduced to the background current in the absence of glucose), owing to the restricted diffusion of glucose, and the I_{pa} of FcCA reduced significantly. This result therefore improves on previously developed biocatalytic swtichable sensors that display relatively high residual currents in the OFF state, limiting the true switchability of the sensor, despite excellent sensing performance in the "ON" state (Parlak et al., 2015b). To characterise

the reversibility of associated bioelectrocatalytic cycling, multiple switching cycles were monitored by DPV (Figure 5D). The I_{pa} of FcCA in the presence of 10 mM glucose remained above 90% in the "ON" state through the cycling experiment, and there was no significant change in peak current in the "OFF" state. Overall, the switching of our device using temperature and pH allowed to regulate the output current in response to glucose by 70–90%. The linear range of our sensor and the associated limit of detection and sensitivity compare favourably to a broad range of GOx sensors reported in the literature, whilst conferring excellent responsiveness and switchable functions (Akkaya et al., 2018; Mishra et al., 2017). Typically, switchable biosensors do not display a combination of high sensitivity, low limit of detection and excellent reproducibility, compared to the behaviour presently reported (Chen et al., 2019a; Liu et al., 2010; Mishra et al., 2017; Parlak et al., 2015a; Yao et al., 2014; Yu et al., 2016). Therefore, we demonstrated the design of a switchable glucose biosensor with an AND logic gate, using precise positioning of an enzyme within a hierarchically structured polymer brush-interface.

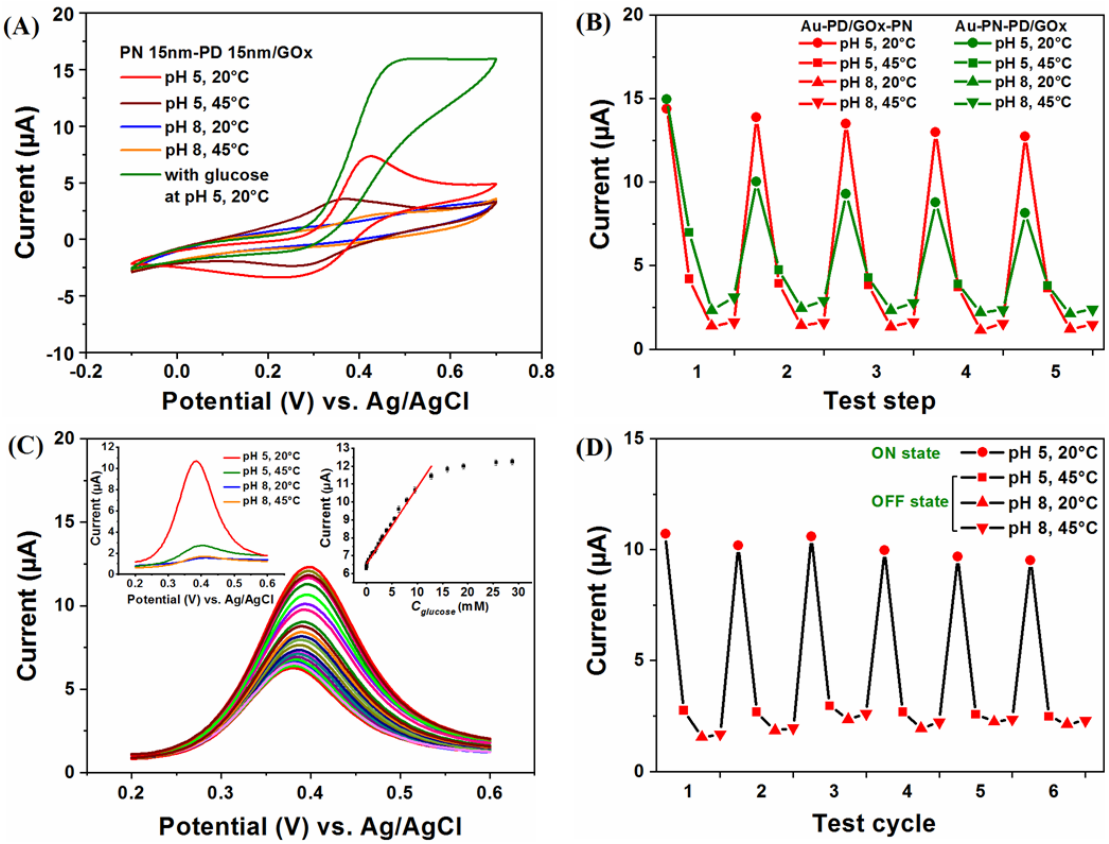

Figure 5. (A) CVs of Au–PNIPAM–*b*–PDMAEMA/GOx (PN–PD/GOx for short in the figure) at a grafting density of 0.33 chains nm^{-2}, with a dry thickness of 15 nm for each block. (B) Dependence of the CV oxidation peak current of FcCA towards 10 mM glucose for PD/GOx–PN and PN–PD/GOx on the cycle number. (C) DPVs of Au–PDMAEMA/GOx–*b*–PNIPAM, in PBS containing 1 mM FcCA at pH 5 and 20ºC, with successive addition of glucose. Inset on the right: the calibration curves for glucose at this electrode. Inset on the left: Responsiveness of this electrode towards pH and temperature in the presence of 10 mM glucose. (D) Dependence of the DPV oxidation peak current of FcCA towards 10 mM glucose on the cycle number. Cycling was carried out in PBS containing 1 mM FcCA at pH 5 and 20ºC, pH 5 and 45ºC, pH 8 and 20ºC, pH 8 and 45ºC, and in the presence of 10 mM glucose at pH 5 and 20ºC. Scan rate: 50 mV s^{-1}.

4. Conclusions

The performance of bioelectrocatalytic logic gates depends on the sensitivity of their response to bioanalytes, the tight control of their responsive behaviour and the ability to retain electroactivity upon environmental cycling. The design of interfaces that achieve such performance has remained elusive, but our results demonstrate that, through the precise positioning of enzymatic catalytic sites, it is possible to achieve repeated cycling between "ON" and "OFF" states whilst displaying high signal-to-noise intensity ratios in a relevant range of bioanalyte concentrations. The ability to engineer polymer brush architectures to control the responsive behaviour of interfaces is well documented, but the ability to entrap enzymes within specific compartments by exploiting the re-initiation of polymer brush growth will enable the precise positioning of a range of other biocatalytic sites within biosensors and logic gate interfaces. The impact of polymer brush architecture (including the chemistry of each block) and the formation of multi-block-copolymer structures may bring further levels of sensitivity and additional responsive behaviours for the design of bioelectrocatalytic interfaces. Although some enzymes may not tolerate the use of hydrophobic solvents, and dehydration, during brush synthesis, fully aqueous polymerisation conditions and flow through cells should enable greater flexibility and the preservation of the catalytic activity of relatively sensitive enzymes that rapidly denature. Therefore the platform proposed opens the door to the design of a new generation of responsive interfaces for bioelectrocatalytic logic gates that may be applied to the fields of biosensing or catalysis.

Credit authorship contribution statement

Fengjin Qu: Methodology, Formal analysis, Writing - original draft, Funding acquisition. **Xiaoyan Ma:** Conceptualization, Writing - review & editing, Supervision, Funding acquisition. **Julien E. Gautrot:** Conceptualization, Supervision, Writing - original draft.

Declaration of competing interest

The authors declare that they have no known competing financial interests or personal relationships that could have appeared to influence the work reported in this paper.

Acknowledgements

We thank the China Scholarship Council (no. 201706290160) and the National Natural Science Foundation of China (no. 51772248) for financial support.

Appendix A. Supplementary data

Supplementary data to this article can be found online at

References

Akkaya, B., Cakiroglu, B., Ozacar, M., 2018. ACS Sustain. Chem. Eng. 6 (3), 3805-3814.

Bokias, G., Staikos, G., Iliopoulos, I., 2000. Polymer 41 (20), 7399-7405.

Cass, A.E.G., Davis, G., Francis, G.D., Hill, H.A.O., Aston, W.J., Higgins, I.J., Plotkin, E.V., Scott, L.D.L., Turner, A.P.F., 1984. Anal. Chem. 56 (4), 667-671.

Chen, C., Zhao, P.C., Ni, M.J., Li, C.Y., Xie, Y.X., Fei, J.J., 2019a. Analyst 144 (6), 1960-1967.

Chen, F., Dong, C., Chen, C., Yin, W.D., Zhai, W., Ma, X.Y., Wei, B., 2019b. Ultrason. Sonochem. 58, 104705-104710.

Chen, Y., Gai, P.P., Xue, J.J., Zhang, J.R., Zhu, J.J., 2015. Biosens. Bioelectron. 74, 142-149.

Gamella, M., Guz, N., Mailloux, S., Pingarron, J.M., Katz, E., 2014. ACS Appl. Mater. Inter. 6 (16), 13349-13354.

Garcia, T.A., Gervasi, C.A., Presa, M.J.R., Otamendi, J.I., Moya, S.E., Azzaroni, O., 2012. J. Phys. Chem. C 116 (26), 13944-13953.

Ishida, N., Biggs, S., 2010. Macromolecules 43 (17), 7269-7276.

Karbarz, M., Gniadek, M., Stojek, Z., 2009. Electroanal. 21 (12), 1363-1368.

Katz, E., Willner, I., 2003. J. Am. Chem. Soc. 125 (22), 6803-6813.

Krishnamoorthy, M., Hakobyan, S., Ramstedt, M., Gautrot, J.E., 2014. Chem. Rev. 114 (21), 10976-11026.

Krishnamoorthy, M., Li, D.Y., Sharili, A.S., Gulin-Sarfraz, T., Rosenholm, J.M., Gautrot, J.E., 2017. Biomacromolecules 18 (12), 4121-4132.

Laloyaux, X., Mathy, B., Nysten, B., Jonas, A.M., 2010. Langmuir 26 (2), 838-847.

Li, D.Y., Xu, L.Z., Wang, J., Gautrot, J.E., 2020. Adv. Healthc. Mater. 2000953.

Liang, J.Y., Yu, X., Yang, T.G., Li, M.L., Shen, L., Jin, Y., Liu, H.Y., 2017. Phys. Chem. Chem. Phys. 19 (33), 22472-22481.

Liu, D., Hu, N.F., 2011. Sensor Actuat B-Chem 156 (2), 645-650.

Liu, D., Liu, H.Y., Hu, N.F., 2010. Electrochim. Acta. 55 (22), 6426-6432.

Minko, S., 2006. Polym. Rev. 46 (4), 397-420.

Mishra, S., Ashaduzzaman, M., Mishra, P., Swart, H.C., Turner, A.P.F., Tiwari, A., 2017. Biosens. Bioelectron. 89, 305-311.

Parlak, O., Ashaduzzaman, M., Kollipara, S.B., Tiwari, A., Turner, A.P.F., 2015a. ACS Appl. Mater. Inter. 7 (43), 23837-23847.

Parlak, O., Turner, A.P.F., Tiwari, A., 2015b. J. Mater. Chem. B 3 (37), 7434-7439.

Plunkett, K.N., Zhu, X., Moore, J.S., Leckband, D.E., 2006. Langmuir 22 (9), 4259-4266.

Privman, M., Tam, T.K., Pita, M., Katz, E., 2009. J. Am. Chem. Soc. 131 (3), 1314-1321.

Qu, F.J., Li, D.Y., Ma, X.Y., Chen, F., Gautrot, J.E., 2019. Biomacromolecules 20 (6), 2218-2229.

Qu, F.J., Ma, X.Y., Zhu, L., Chen, F., 2017. Electrochem. Commun. 77, 49-53.

Rosenthal, A., Rauch, S., Eichhorn, K.J., Stamm, M., Uhlmann, P., 2018. Colloid. Surface. B 171, 351-357.

Schmidt, S., Motschmann, H., Hellweg, T., von Klitzing, R., 2008. Polymer 49 (3), 749-756.

Wang, L., Lian, W.J., Yao, H.Q., Liu, H.Y., 2015. ACS Appl. Mater. Inter. 7 (9), 5168-5176.

Wang, L., Shao, H., Lu, X., Wang, W., Zhang, J.R., Song, R.B., Zhu, J.J., 2018. Chem. Sci. 9 (45), 8482-8491.

Wei, Q., Becherer, T., Angioletti-Uberti, S., Dzubiella, J., Wischke, C., Neffe, A.T., Lendlein, A., Ballauff, M., Haag, R., 2014. Angew. Chem. Int. Edit. 53 (31), 8004-8031.

Wilson, R., Turner, A.P.F., 1992. Biosens. Bioelectron. 7, 165-185.

Xue, C.Y., Yonet-Tanyeri, N., Brouette, N., Sferrazza, M., Braun, P.V., Leckband, D.E., 2011. Langmuir 27 (14), 8810-8818.

Yao, H., Lin, L., Wang, P., Liu, H., 2014. Appl. Biochem. Biotechnol. 173 (8), 2005-2018.

Yu, X., Lian, W.J., Zhang, J.N., Liu, H.Y., 2016. Biosens. Bioelectron. 80, 631-639.

Zakharchenko, A., Guz, N., Laradji, A.M., Katz, E., Minko, S., 2018. Nat. Catal. 1 (1), 73-81.

Zang, Y., Zhu, H.M., Xue, H.G., 2018. Electrochim. Acta. 259, 676-684.

Zhang, J.J., Ma, W.J., He, X.P., Tian, H., 2017. ACS Appl. Mater. Inter. 9 (10), 8498-8507.

Zhang, K.N., Liang, Y., Liu, D., Liu, H.Y., 2012. Sensor. Actuat. B-Chem. 173, 367-376.

Zhou, J.H., Liu, J., Wang, G., Lu, X.B., Wen, Z.H., Li, J.H., 2007. Adv. Funct. Mater. 17 (16), 3377-3382.

Zoppe, J.O., Ataman, N.C., Mocny, P., Wang, J., Moraes, J., Klok, H.A., 2017. Chem. Rev. 117 (3), 1105-1318.